Int J Adv Manuf Technol (2017) 91:13–24
DOI 10.1007/s00170-016-9753-3

ORIGINAL ARTICLE

Modeling and experiment of surface error for large-aperture aspheric SiC mirror based on residual height and wheel wear

Chen Li[1] · **Feihu Zhang**[1] · **Zhaokai Ma**[1] · **Ye Ding**[1]

Received: 12 September 2016 / Accepted: 7 November 2016 / Published online: 15 November 2016

Abstract In the grinding process of large-aperture aspheric silicon carbide mirror, the wear of grinding wheel affects the surface accuracy seriously due to high hardness of silicon carbide and large diameter of aspheric mirror. Therefore, establishing surface error model of large-aperture aspheric silicon carbide mirror taking the wear of grinding wheel into account is of great significance to improve the processing quality and the imaging quality of aspheric mirror. The spiral grinding method is chosen to grind large-aperture aspheric SiC mirror in this work. The surface error of large-aperture aspheric silicon carbide mirror is established based on residual height and radial wear of grinding wheel using the grinding ratio as a bridge. The influence of grinding parameters on surface error is analyzed based on theoretical model. The results show that surface error increases with the increase of the rotation radius of workpiece and feed velocity of wheel, while it decreases with the increase of rotation velocity of workpiece and arc radius of wheel. The influence of the rotation velocity of workpiece and feed velocity of wheel is greater than that of the rotation radius of workpiece and arc radius of wheel. The regression equation of grinding ratio is established through grinding experiment, and the correlation coefficient is 0.9774 which verifies the reliability of the regression equation. Furthermore, the complete formula of surface error is acquired based on regression equation of grinding ratio. Finally, the grinding experiment of large-aperture aspheric silicon carbide mirror is carried out on the five-axis NC milling and grinding machine tool of HZ-091 type, and the error between measured value of grinding experiment and prediction value of theoretical model is less than 20%, which indicates that the theoretical model is reliable.

Keywords Surface error · Large aperture · Aspheric mirror · Wear of grinding wheel

1 Introduction

With the development of space optical technology, people put forward higher and higher requirements for the imaging quality of mirror. Long focal length and large diameter become the important means to improve the resolution of the remote sensing system [1, 2]. Compared to spherical surfaces, the utilization of aspheric surfaces in optical systems brings advantages such as better optical performance, reducing the number of optical elements, reducing system weight, and greater design flexibility [3, 4]. Therefore, the manufacture of large-aperture aspheric mirror becomes the mainstream tendency for development of mirror [5, 6].

Silicon carbide ceramics are widely used in the field of aeronautics and astronautics, electrical and electronic engineering, space optics technology, and automobile manufacturing over the last three decades with their excellent physical and mechanical characteristic, such as low density, high strength, chemical stability, low coefficient of thermal expansion, and so on [7, 8]. In particular,

✉ Chen Li
hit_chenli@163.com

Feihu Zhang
zhangfh@hit.edu.cn

Zhaokai Ma
mazhaokai2014@163.com

Ye Ding
dy1992hit@163.com

1 School of Mechatronics Engineering, Harbin Institute of Technology, Harbin 150001, China

silicon carbide ceramics has turned into the primary material for large-aperture mirror. It has been a hot issue to efficiently manufacture the high-precision large-aperture aspheric silicon carbide mirror so far. Many scholars have demonstrated strong interests on the processing of large-aperture aspheric silicon carbide mirror. Jiang et al. [9] established a unified 3D geometric model of toric wheel workpiece contact area whose boundaries was based on the local geometric properties of the wheel and the workpiece at the grinding point. Based on the force distribution within the contact area and the coupled relationship between grinding force and wheel deformation, the specific grinding energy and the final predicted grinding force were obtained iteratively. Finally, the proposed methods were validated through grinding experiments. Xie et al. [10] investigated the ductile-mode grinding in connection with elliptical torus eccentricity and grinding variables, which contributed to decreasing the grain cutting depth to the critical cutting depth without nanometer-scale depth of cut, and further leading to efficient ductile-mode grinding. Agarwal [11] conducted experiments in order to study the effect of various parameters such as depth of cut, table feed, size and density of grit on the metal removal rate, surface roughness, and surface and subsurface damage. He developed the mathematical models using the data obtained experimentally considering the significant parameters only and optimized the ceramic grinding process with multiple objectives based on the genetic algorithm. Zhang et al. [12] studied the material removal mechanism and friction behavior of reaction-bonded silicon carbide ceramic based on the nanoscratch test using Berkovich and sphere indenters, and they found that the plowing friction coefficient played a significant role in the plastic processing stage of RBSC using the Berkovich indenter. Moreover, the fluctuation of the cutting force and friction coefficient was analyzed to be caused by the specific microstructure of the material. From the previous work, it can be summarized that previous researches mainly put their focus on grinding force [9], surface integrity and subsurface damage [10], material removal rate [11], and material removal mechanism of silicon carbide ceramics [12] about mirror manufacture.

As one of the important evaluating indicators for the processing quality of mirror, surface error generated in the grinding process will reduce the accuracy and efficiency of the workpiece. Therefore, researchers have carried out beneficial explorations and large number of experiments to improve the surface accuracy of large-aperture mirror, such as establishing motion error model of machine tools and providing compensation [13–15], dressing grinding wheel on line [16], innovating efficiency grinding trajectory [17], improving the detection accuracy, and providing compensation [18]. Ferreira et al. [13] developed a model for quasistatic errors of machine tools on the basis for a viable error compensation scheme, the model for error compensation and the parameter estimation for updating the model. Furthermore, he stated that the parameters for this model could be estimated by the observation of a few error vectors in the machine's workspace and verified the validity of the approach by the experiment. Chatterjee [14] reported a spatial error model of multiaxis machine tools with expression application of the vector chain. The analysis of data from the model, post-process measurements, and static geometric accuracy machine tool characterization parameters indicated significant shifts in machine performance under actual cutting conditions. Lin et al. [15] established the surface accuracy model of large size of axisymmetric aspheric using the theory of rigid body kinematics based on grating parallel grinding method, in which the influence degree of the monomial error was analyzed. The results of error compensation showed the reliability of surface accuracy model. Rahman [16] et al. developed an on-machine profile measurement system referring to coordinate measuring machine (CMM) principle to check the profile radius of the ground surface. They applied software compensation in ELID grinding of an aspheric surface in order to compensate the wheel wear until the measured surface profile machined on BK7 glass reaches within tolerable limit. Kuriyagawa et al. [17] designed an ultra-precise grinding system based on a new grinding technique called the "Arc Envelope Grinding Method (AEGM)" to grind aspheric ceramic mirrors. And the aspheric silicon carbide mirrors of 100 mm in diameter were successfully ground using the AEGM. The form error after the first grinding without any compensation was less than 1.8 μm, and the roughness *Ra* was 10 nm. Xiao et al. [18] proposed an alternative scanning deflectometry method for the measurement of large aspheric optical surfaces, wherein a rotation stage was incorporated to increase the measurement range of the high-accuracy autocollimators used to measure small angles. The verification experiment results showed that for the measurements of large aspheric surfaces with large slope changes, 10 nm repeatability, was achievable under the suitable conditions.

Establishing the surface error model, exploring the relationship between surface error and grinding parameters, and proposing compensation strategy provide new ideals for the high efficiency and precision machining of large-aperture aspheric SiC mirror. Some prediction models of surface error for aspheric mirror were established, and the influence of grinding parameters on surface error is analyzed [19, 20]. But these models did not take the wear of grinding wheel into consideration, especially in the large-aperture aspheric silicon carbide mirror. As we all know, the grinding wheel wears seriously in the grinding process for the high hardness of silicon carbide and large-aperture of mirror [21, 22]. So developing the surface error model taking the wear of grinding wheel into account is of great significance for improving the imaging quality of aspheric mirror.

Comparing with reciprocating grinding method, spiral grinding method has many advantages in the grinding process of aspheric mirror, such as high uniformity of grinding trajectory and high surface accuracy [23]. So spiral grinding method is chosen to grind the large-aperture aspheric SiC mirror in this work. The surface error model of large-aperture aspheric SiC mirror is developed based on the residual height and radial wear of grinding wheel using the grinding ratio as a bridge. The influence of grinding parameters on surface error is analyzed based on the model. The grinding ratio regression equation is established through the grinding ratio experiment, and the complete formula of the surface error is obtained. Finally, the theoretical model of surface error is verified by the grinding experiment of the large-aperture aspheric SiC mirror.

2 Modeling of aspheric surface error based on residual height and wear of grinding wheel

2.1 Aspheric surface equation and related geometric parameters

In the grinding process of mirror, the aspheric surface equation is shown in Eq. (1).

$$z = \frac{x^2}{R_0 + \sqrt{R_0^2 - (1-e^2)x^2}} \tag{1}$$

where z is the height coordinate of aspheric surface, x is the rotation radius of workpiece, R_0 is the curvature radius when x is 0, and e is the eccentricity of aspheric surface.

As shown in Fig. 1, the value of e^2 determines the shape of conic section.

According to aspheric surface equation (Eq. (1)), the slope of the tangent for any point at quadratic revolution aspheric surface is shown in Eq. (2).

$$\dot{z} = \tan\beta = \frac{x}{\sqrt{R_0^2 - (1-e^2)x^2}} \tag{2}$$

where $\tan\beta$ is the slope when rotation radius of workpiece is x, rad.

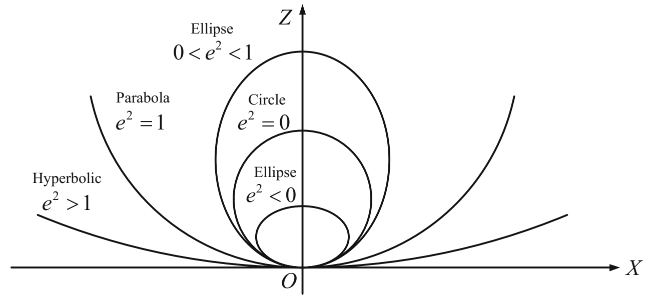

Fig. 1 The conic section in different eccentricities

The second derivative of z can be acquired from Eq. (2).

$$\ddot{z} = \frac{x}{\left(R_0^2 - (1-e^2)x^2\right)^{3/2}} \tag{3}$$

Furthermore, the parameters $\cos\beta$, $\sin\beta$, and $\sec^2\beta$ can be obtained from Eq. (2).

$$\cos\beta = \frac{\sqrt{R_0^2 - (1-e^2)x^2}}{\sqrt{R_0^2 + e^2x^2}} \tag{4}$$

$$\sin\beta = \frac{x}{\sqrt{R_0^2 + e^2x^2}} \tag{5}$$

$$\sec^2\beta = \frac{R_0^2 + e^2x^2}{R_0^2 - (1-e^2)x^2} \tag{6}$$

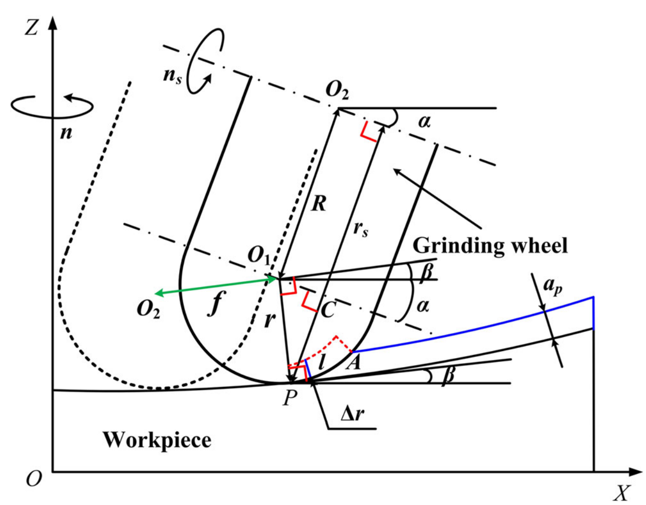

Fig. 2 Diagram of arc grinding wheel wear

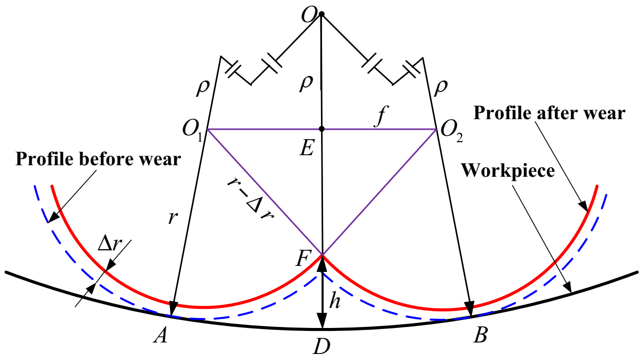

Fig. 3 Diagram of residual height

According to the principle of differential geometry, the radius of the principal curvature of any point on the meridian is shown in Eq. (7):

$$\rho=\frac{\left(1+\dot{z}^{2}\right)^{3/2}}{|\ddot{z}|} \tag{7}$$

where ρ is the radius of principal curvature.

Take Eq. (3) into Eq. (7) and the complete formula of radius of the principal curvature can be acquired.

$$\rho=\frac{\left(e^{2}x^{2}+R_{0}^{2}\right)^{3/2}}{R_{0}^{2}} \tag{8}$$

2.2 Wear calculation of arc grinding wheel

The process of arc wheel grinding aspheric surface which adopts the spiral grinding method is shown in Fig. 2. The contact point of grinding wheel and the workpiece varies in different rotation weeks, and the corresponding length of contact arc also varies in different rotation weeks. Because the grinding depth in the grinding process of large-aperture mirror is small, and the feed velocity of grinding wheel along the direction of the generatrix are very low. Therefore, in order to simplify the calculation, the following assumptions could be given in this work:

1. Diamond abrasives are evenly distributed on each grinding wheel layer.
2. The contact region between grinding wheel and workpiece in the section of generatrix is a section of arc.
3. Grinding ratio remains constant in stable grinding stage and is only determined by grinding parameters.
4. The wheel wear of each contact arc is uniform.

In the process of arc wheel grinding aspheric surface, the wear diagram of workpiece is shown in Fig. 2. R is the radius of basic circle, r is the radius of grinding wheel, r_s is the rotation radius of the grinding wheel at the contact point of grinding wheel and workpiece, α is the included angle between central line of grinding wheel rotating and horizontal line, β is the included angle between the tangent at contact point P and the horizontal line, l is the length of contact arc between arc grinding wheel with workpiece, Δr is the radial wear depth of grinding wheel at the contact point P, a_p is the grinding depth, and f is the distance of two adjacent wheel centers.

According to assumption that the wheel wear of each contact arc is uniform and the radial wear depth is Δr, the actual grinding depth is (a_p-Δr). The trajectory length of grinding wheel is $2\pi x$ and feed distance grinding wheel is equal to the distance of two adjacent wheel centers during workpiece rotating a week. Therefore, when rotation radius is x, the material removal volume V_w during workpiece rotating a week is shown in Eq. (9).

$$V_w=2\pi x\cdot\left(a_p-\Delta r\right)\cdot f \tag{9}$$

The sectional area of wear volume is $l\Delta r$, and the wear length of grinding wheel is $2\pi r_s$. Therefore, when rotation radius is x, the wear volume of arc grinding wheel V_s during

Fig. 4 Diagram surface profile in meridian section (**a**) and surface error (**b**)

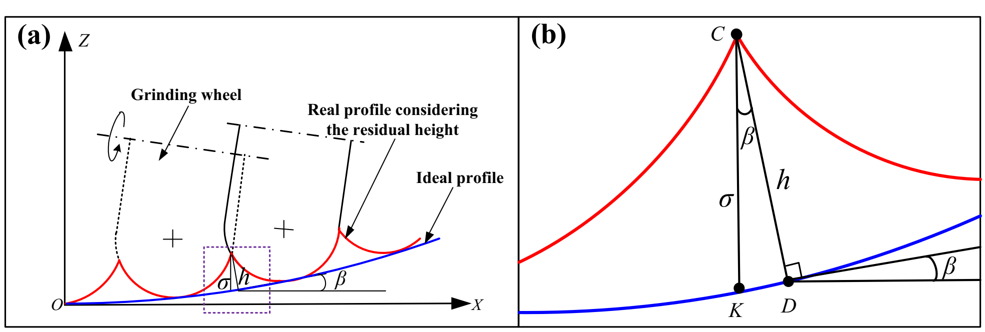

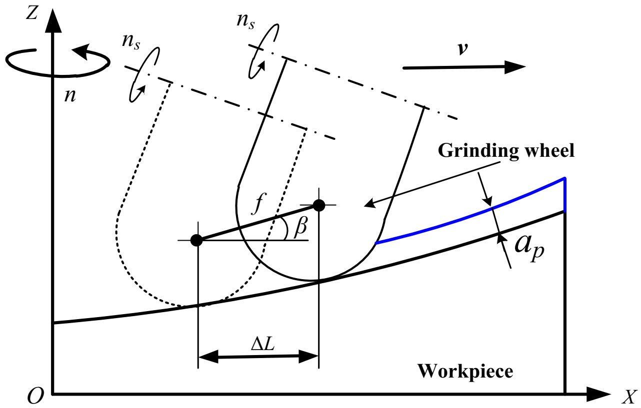

Fig. 5 Diagram of two adjacent grinding wheel positions in radial direction

workpiece rotating a week is the product of sectional area of wear volume and wear length of grinding wheel.

$$V_s = 2{\cdot}\pi{\cdot}r_s{\cdot}l{\cdot}\Delta r \tag{10}$$

As shown in Fig. 2, $\angle O_1PC + \angle PO_1C = \pi/2$ and $\alpha + \beta + \angle PO_1C = \pi/2$. Therefore, $\angle O_1PC = \alpha + \beta$. The rotation radius of the grinding wheel at the contact point of grinding wheel and workpiece can be calculated by the radius of basic circle R and the radius of grinding wheel r.

$$r_s = R + r{\cdot}\cos(\angle O_1PC) = R + r{\cdot}\cos(\alpha + \beta) \tag{11}$$

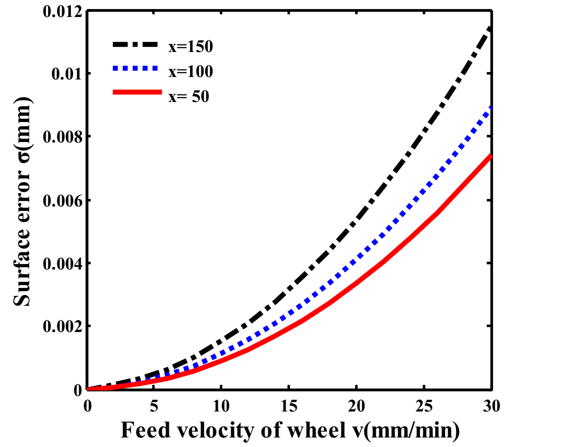

Fig. 7 Relationship between surface error and feed velocity of wheel (n = 30 r/min, r = 20 mm, R = 40 mm, α = 30°)

Similar to cylindrical grinding, the contact arc length l between the arc grinding wheel and workpiece can be calculated by the Eq. (12) [24]:

$$l = \sqrt{\frac{2{\cdot}a_p{\cdot}r}{1-r/\rho}} \tag{12}$$

In the stable stage of grinding, the grinding ratio is a constant value. So material removal volume V_w and the wear volume of arc grinding wheel V_s fit the Eq. (13).

$$G = \frac{V_w}{V_s} \tag{13}$$

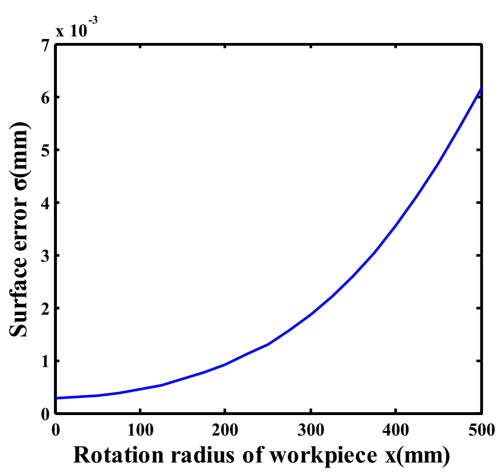

Fig. 6 Relationship between surface error and rotation radius of workpiece (v = 6 mm/min, n = 30 r/min, r = 20 mm, R = 40 mm, α = 30°)

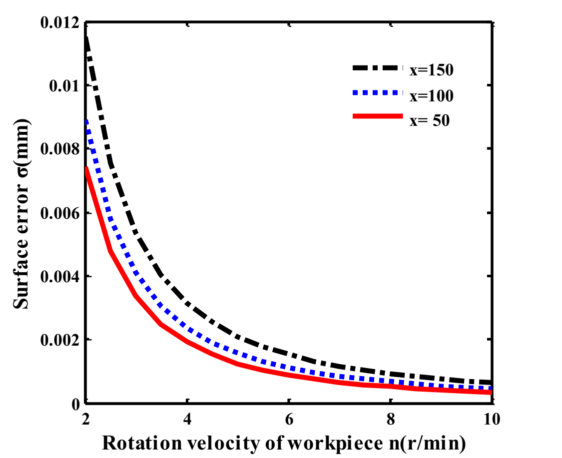

Fig. 8 Relationship between surface error and rotation velocity of workpiece (v = 2 mm/min, r = 20 mm, R = 40 mm, α = 30°)

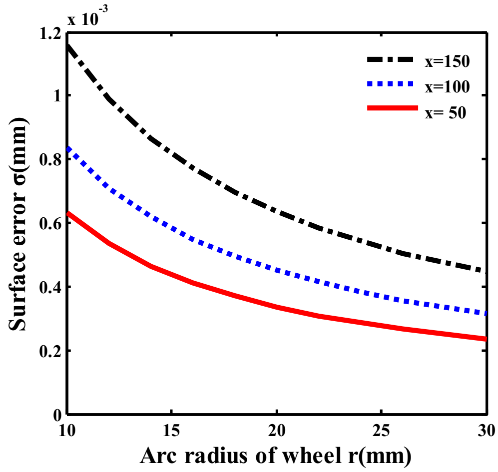

Fig. 9 Relationship between surface error and arc radius of wheel (v = 6 mm/min, n = 30 r/min, R = 40 mm, α = 30°)

Taking Eqs. (9)~(12) into Eq. (13), the following equation is obtained:

$$2\cdot\pi\cdot x\cdot\left(a_p-\Delta r\right)\cdot f = 2\cdot\pi\cdot G\cdot\Delta r\cdot(R+r\cdot\cos(\alpha+\beta))\sqrt{\frac{2\cdot a_p\cdot r}{1-r/\rho}} \tag{14}$$

The radial wear depth of grinding wheel Δr is acquired by rearranging Eq. (14).

$$\Delta r = \frac{a_p\cdot f\cdot x}{f\cdot x+G\cdot(R+r\cdot\cos(\alpha+\beta))\cdot\sqrt{2\cdot a_p\cdot r\Big/(1-r/\rho)}} \tag{15}$$

where $\rho=\frac{\left(e^2x^2+R_0^2\right)^{3/2}}{R_0^2}$, and $\cos(\alpha+\beta)$ can be calculated by Eqs. (4) and (5).

$$\cos(\alpha+\beta)=\cos\alpha\cdot\cos\beta-\sin\alpha\cdot\sin\beta=\frac{\cos\alpha\sqrt{R_0^2-(1-e^2)x^2}-x\sin\alpha}{\sqrt{R_0^2+e^2x^2}} \tag{16}$$

Table 1 The physical properties of RB-SiC ceramics

Material	Elasticity modulus (GPa)	Fracture toughness (MPa·m$^{1/2}$)	Poisson ratio	Coefficient of thermal expansion (×10^{-6}/K)	Density (kg/m^3)
RB-SiC	420	0.602	0.16	4.4	2740

Table 2 Parameters of grinding wheel in grinding ratio

Diameter (mm)	Grain size	Binding agent	Width (mm)	Concentration
250, 300	120#	Metal	10	100%

2.3 Modeling of residual height for aspheric surface

The diagram of residual height in the grinding process of aspheric surface is shown in Fig. 3. The contact region between grinding wheel and workpiece in the section of generatrix is a small section of arc. The residual height is deformed by the two adjacent contact arcs in the grinding layer. A and B are two contact points of adjacent grinding trajectory. The curvature radius in contact point A and that in contact point B can be considered equal, and they are denoted by ρ. f is the distance of two grinding wheel centers of adjacent grinding trajectory, and Δr is the radial wear depth of grinding wheel.

As shown in Fig. 3, the residual height h can be calculated by the parameters ρ, $\overline{OE}$, and $\overline{EF}$:

$$h=\rho-\overline{OE}-\overline{EF} \tag{17}$$

Because $\angle O_1OE$ and $\angle O_2OE$ are very small, $\angle O_1EO$ and $\angle O_2EO$ can be regarded as right angle. Therefore, $\overline{OE}$ and $\overline{EF}$ can be calculated based on the geometrical relationship.

$$\overline{OE}=\sqrt{(\rho-r)^2-\left(\frac{f}{2}\right)^2} \tag{18}$$

$$\overline{EF}=\sqrt{(r-\Delta r)^2-\left(\frac{f}{2}\right)^2} \tag{19}$$

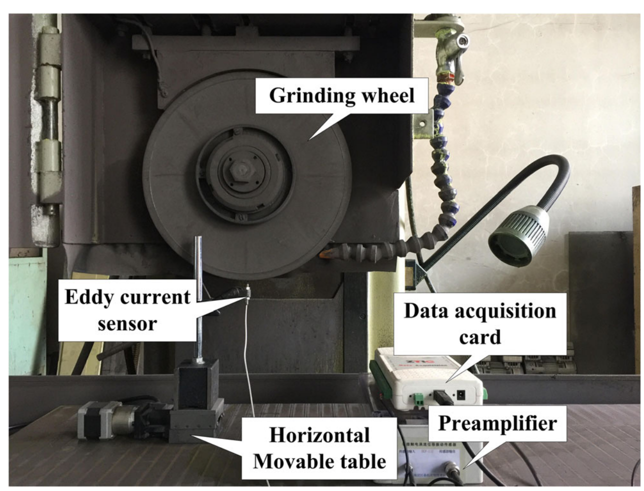

Fig. 10 Measuring device for wear volume of grinding wheel

Table 3 Experiment parameters and results of grinding ratio

No.	Grinding velocity of wheel v_s (m/s)	Grinding depth a_p (μm)	Feed velocity v (mm/min)	Grinding ratio G
1	19.63	20	102	94.35
2	19.63	30	248	83.35
3	23.56	30	102	99.00
4	23.56	20	248	97.19
5	19.63	20	248	85.52
6	19.63	30	102	88.18
7	23.56	20	102	103.26
8	23.56	30	248	89.72

Taking the Eqs. (18) and (19) into Eq. (17), the formula of residual height h is shown in Eq. (20).

$$h=\rho-\sqrt{(\rho-r)^2-\left(\frac{f}{2}\right)^2}-\sqrt{(r-\Delta r)^2-\left(\frac{f}{2}\right)^2} \tag{20}$$

$$\text{Where,}\begin{cases}\Delta r=\dfrac{a_p\cdot f\cdot x}{f\cdot x+G\cdot(R+r\cdot\cos(\alpha+\beta))\cdot\sqrt{2\cdot a_p\cdot r\Big/\left(1-r\big/\rho\right)}}\\ \cos(\alpha+\beta)=\dfrac{\cos\alpha\sqrt{R_0^2-(1-e^2)x^2}-x\sin\alpha}{\sqrt{R_0^2+e^2x^2}}\\ \rho=\dfrac{\left(e^2x^2+R_0^2\right)^{3/2}}{R_0^2}\end{cases}$$

.

When $\Delta r = 0$, the formula of residual height without taking the wheel wear into account is shown in Eq. (21).

$$h=\frac{\left(e^2x^2+R_0^2\right)^{3/2}}{R_0^2}-\sqrt{\left(\frac{\left(e^2x^2+R_0^2\right)^{3/2}}{R_0^2}-r\right)^2-\left(\frac{f}{2}\right)^2}-\sqrt{r^2-\left(\frac{f}{2}\right)^2} \tag{21}$$

2.4 Modeling of surface error based on residual height

The surface error σ is the difference between the actual profile and the theoretical profile in the vertical direction, which can be calculated based on the residual height and radial wear of grinding wheel in spiral grinding of mirror. The ideal profile and real profile in meridian section are shown in Fig. 4a. The residual height deformed by the two adjacent contact arcs in the grinding layer affects the surface error, and the relationship between residual height and surface error is shown in Fig. 4b.

As shown in Fig. 4b, $\overline{DK}$ can be regarded as a straight line because it is very short. And the surface error is obtained by the residual height.

$$\sigma=\frac{h}{\cos\beta} \tag{22}$$

Taking Eq. (20) into Eq. (22), the following formula can be obtained:

$$\sigma=\frac{\rho-\sqrt{(\rho-r)^2-\left(\frac{f}{2}\right)^2}-\sqrt{(r-\Delta r)^2-\left(\frac{f}{2}\right)^2}}{\cos\beta} \tag{23}$$

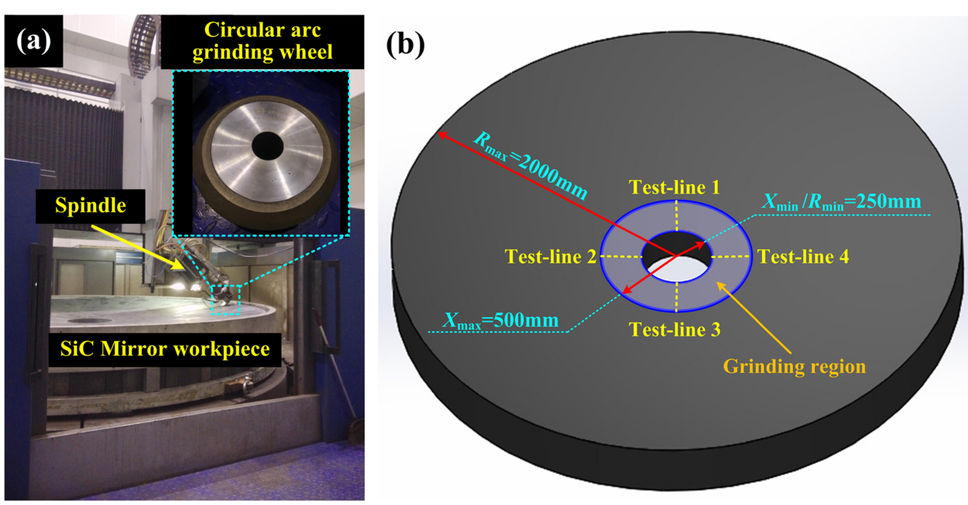

Fig. 11 Five-axis NC milling and grinding machine tool of HZ-091 type (**a**) and mirror workpiece (**b**)

Table 4 Parameters of grinding wheel in mirror grinding

Diameter of wheel d_s (mm)	Arc radius r (mm)	Basic circle radius R (mm)	Width B (mm)	Grain size	Concentration	Binding agent
225	146.86	0	30	120#	100%	Metal

where

$$\begin{cases} \Delta r = \dfrac{a_p \cdot f \cdot x}{f \cdot x + G \cdot (R + r \cdot \cos(\alpha+\beta)) \cdot \sqrt{2 \cdot a_p \cdot r/(1-r/\rho)}} \\ \cos(\alpha+\beta) = \dfrac{\cos\alpha \sqrt{R_0^2 - (1-e^2)x^2} - x\sin\alpha}{\sqrt{R_0^2 + e^2 x^2}} \\ \rho = \dfrac{\left(e^2x^2 + R_0^2\right)^{3/2}}{R_0^2} \\ \cos\beta = \dfrac{\sqrt{R_0^2 - (1-e^2)x^2}}{\sqrt{R_0^2 + e^2x^2}} \end{cases}$$

.

2.5 Influence of grinding parameters on surface error

In order to determine the suitable grinding parameters and improve the surface accuracy, it is necessary to analyze the influence of grinding parameters on surface error. In grinding process of large-aperture mirror, the feed method of grinding wheel in radial direction is shown in Fig. 5. v is the feed velocity of grinding wheel (mm/min). n is the rotation velocity of workpiece (r/min). n_s is the rotation velocity of grinding wheel (r/min).

The feed distance of grinding wheel during the workpiece rotating a week is ΔL.

$$\Delta L = \frac{v}{n} \tag{24}$$

The relationship between distance of two adjacent wheel centers f and ΔL is shown in Eq. (25).

$$f = \frac{\Delta L}{\cos\beta} \tag{25}$$

The theoretical model of surface error is acquired taking Eqs. (24) and (25) into Eq. (23).

$$\sigma = \frac{\rho - \sqrt{(\rho-r)^2 - \left(\frac{v}{2 \cdot n \cdot \cos\beta}\right)^2} - \sqrt{(r-\Delta r)^2 - \left(\frac{v}{2 \cdot n \cdot \cos\beta}\right)^2}}{\cos\beta} \tag{26}$$

where

$$\begin{cases} \Delta r = \dfrac{a_p \cdot f \cdot x}{f \cdot x + G \cdot (R + r \cdot \cos(\alpha+\beta)) \cdot \sqrt{2 \cdot a_p \cdot r/(1-r/\rho)}} \\ \cos(\alpha+\beta) = \dfrac{\cos\alpha \sqrt{R_0^2 - (1-e^2)x^2} - x\sin\alpha}{\sqrt{R_0^2 + e^2 x^2}} \\ \rho = \dfrac{\left(e^2x^2 + R_0^2\right)^{3/2}}{R_0^2} \\ \cos\beta = \dfrac{\sqrt{R_0^2 - (1-e^2)x^2}}{\sqrt{R_0^2 + e^2x^2}} \end{cases}$$

.

2.5.1 Influence of rotation radius of workpiece on surface error

The aspheric parameters and grinding parameters in simulation calculation are chosen as follows: $e^2 = 1$, $R_0 = 250$ mm, $G = 100$, and $a_p = 0.03$ mm. The relationship between surface error σ and rotation radius of workpiece x is shown in Fig. 6 which shows that the surface error increases with the increase of the rotation radius of workpiece. The increase of surface error results from that the radial wear of grinding wheel increases causing the increase of residual height.

Table 5 Aspheric parameters of grinding

Curvature radius R_0 (mm)	Eccentricity ratio e^2	Minimum rotation radius $X_{\min}$ (mm)	Maximum rotation radius $X_{\max}$ (mm)
12,000	1	250	500

Table 6 Processing parameters in mirror grinding

Rotation velocity of wheel n_s (r/min)	Feed velocity v (mm/min)	Rotation velocity of workpiece n (r/min)	Grinding depth a_p (μm)
3500	0.6	0.2	20

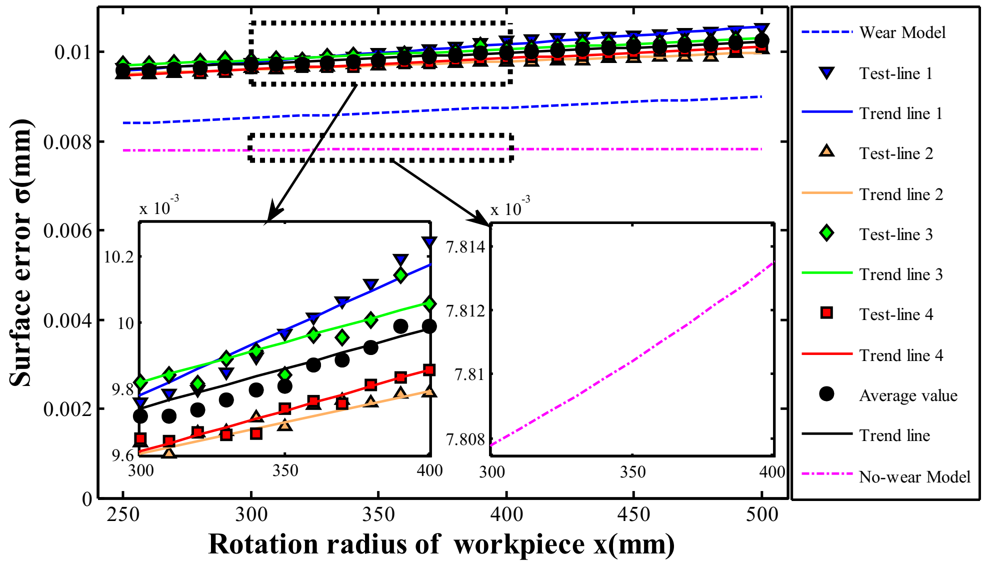

Fig. 12 The experiment results and theoretical prediction values of surface error

2.5.2 Influence of feed velocity of wheel on surface error

The partial derivative of Eq. (26) to feed velocity of grinding wheel v is shown in Eq. (27).

$$\frac{\partial\sigma}{\partial v}=\frac{v}{4n^2\cdot(\cos\beta)^3\cdot\sqrt{(\rho-r)^2-\left(\frac{v}{2n\cos\beta}\right)^2}}+\frac{v}{4n^2\cdot(\cos\beta)^3\cdot\sqrt{(r-\Delta r)^2-\left(\frac{v}{2n\cos\beta}\right)^2}} \quad (27)$$

Because β is an acute angle, so $\cos\beta > 0$. Obviously, $\frac{\partial\sigma}{\partial v}\geq 0$, which indicates that the surface error is positively correlated with the feed velocity of grinding wheel. The relationship between surface error σ and feed velocity of wheel v is shown in Fig. 7, which showed that the surface error increases with the increase of feed velocity. Therefore, the small feed velocity should be applied in grinding process to guarantee the high surface accuracy.

2.5.3 Influence of rotation velocity of workpiece on surface error

The partial derivative of Eq. (26) to rotation velocity of workpiece n is shown in Eq. (28).

$$\frac{\partial\sigma}{\partial n}=-\left(\frac{v^2}{4n^3\cdot(\cos\beta)^3\cdot\sqrt{(\rho-r)^2-\left(\frac{v}{2n\cos\beta}\right)^2}}+\frac{v^2}{4n^3\cdot(\cos\beta)^3\cdot\sqrt{(r-\Delta r)^2-\left(\frac{v}{2n\cos\beta}\right)^2}}\right) \quad (28)$$

Obviously, $\frac{\partial\sigma}{\partial n}\leq 0$, which indicates the rotation velocity of workpiece is negatively correlated with the surface error. As shown in Fig. 8, the surface error decreases with the increase of rotation velocity of workpiece. Therefore, rotation velocity of workpiece should be improved under the premise of the reliability of mechanical system.

2.5.4 Influence of arc radius of wheel on surface error

The partial derivative of Eq. (26) to arc radius of wheel r is shown in Eq. (29).

$$\frac{\partial\sigma}{\partial r}=\frac{\rho-r}{\cos\beta\cdot\sqrt{(\rho-r)^2-\left(\frac{v}{2n\cos\beta}\right)^2}}-\frac{(r-\Delta r)\cdot\left(1+\frac{a_p\cdot f\cdot G\cdot\cos(\alpha+\beta)\cdot\sqrt{2\cdot a_p\cdot r/(1-r/\rho)}\cdot x}{\left(f\cdot x+G\cdot(R+r\cdot\cos(\alpha+\beta))\cdot\sqrt{2\cdot a_p\cdot r/(1-r/\rho)}\right)^2}\right)}{\cos\beta\cdot\sqrt{(r-\Delta r)^2-\left(\frac{v}{2n\cos\beta}\right)^2}} \quad (29)$$

Obviously, $\frac{\partial\sigma}{\partial r}\leq 0$, which indicates the radius of grinding wheel is negatively correlated with the surface error. As shown in Fig. 9, the surface error decreases with the increase of radius of grinding wheel. Therefore, the larger arc radius of grinding wheel should be chosen to guarantee the surface accuracy of the mirror.

3 Experiment and verification of surface error for large-aperture aspheric SiC mirror

3.1 Grinding ratio experiment and establishment of regression equation

As shown in Eq. (23), the grinding ratio G should be solved to obtain the complete theoretical model of surface error. Therefore, the grinding ratio experiment is carried out on the precision horizontal axis surface grinder of type MM7132A to solve the regression equation of grinding ratio. The material of workpiece is reaction-bonded silicon carbide (RB-SiC) whose physical properties is shown in Table 1, and the content of Si is 10% in RB-SiC ceramics. The size of workpiece is Φ135 mm × 15 mm. The parameters of grinding wheel in grinding ratio are shown in Table 2.

As shown in Fig. 10, the eddy current sensor is employed to measure the diameter of metal-bonded diamond grinding wheel. The measured data are fitted by the circle equation, and the diameter before grinding and that after grinding are obtained. The difference between the diameter before grinding and that after grinding is the radial wear of grinding wheel. Each group of data is measured ten times, and the average value is chosen as final results. The removal volume of SiC ceramics is measured by micrometer.

The experiment parameters and results of grinding ratio are given in Table 3.

The grinding ratio is a constant value in the stable grinding stage for SiC ceramics, and it is related to process parameters. Therefore, the empirical formula of grinding ratio is established using the process parameters as variable.

$$G = k \cdot v_s^a \cdot a_p^b \cdot v^c \tag{30}$$

where k, a, b, and c are undetermined coefficients.

The undetermined coefficients, a, b, c and k, can be obtained by the multiple linear regression method based on the experiment data in Table 2: $a = 0.5577$, $b = -0.1327$, $c = -0.0882$, and $k = 15.9404$. The empirical formula of grinding ratio is obtained in Eq. (31).

$$G = 15.9404 \cdot v_s^{0.5577} \cdot a_p^{-0.1327} \cdot v^{-0.0882} \tag{31}$$

The correlation coefficient is 0.9774 and is close to 1, which indicates that the model is reliable.

Taking Eq. (31) into Eq. (15), the complete equation of radial wear of grinding wheel Δr is acquired.

$$\Delta r = \frac{a_p \cdot f \cdot x}{f \cdot x + 15.9404 \cdot v_s^{0.5577} \cdot a_p^{-0.1327} \cdot v^{-0.0882} (R + r \cdot \cos(\alpha + \beta)) \sqrt{2 a_p \cdot r / (1 - r/\rho)}} \tag{32}$$

3.2 Verification of surface error for large-aperture aspheric SiC mirror

In order to verify the reliable of surface error theoretical model for large-aperture aspheric SiC mirror, the grinding experiment is carried out on the five-axis NC milling and grinding machine tool of HZ-091 type (Fig. 11a). The maximum velocity of spindle rotation of machine tool is 8000 r/min, and the displacement accuracy of machine tool in the directions of x, y, and z is 1 μm. As shown in Fig. 11b, the radius of mirror blank is 2000 mm and the radius of inner hole is 250 mm. A part of the aspheric surface is chosen as the grinding region in the grinding process because it would cost lots of time in grinding process of entire aspheric mirror (the range of rotation radius of workpiece is 250~500 mm in grinding process). And four generatrices of the aspheric surface mirror are test.

The metal-bonded diamond arc grinding wheel is used in the grinding experiment of large-aperture aspheric SiC mirror, and the size and parameters of grinding wheel are shown in Table 4.

Aspheric surface equation is $z = \frac{x^2}{R_0 + \sqrt{R_0{}^2 - (1 - e^2) x^2}}$ and the complete parameters are shown in Table 5.

The processing parameters of aspheric surface in mirror grinding are shown in Table 6.

The three-coordinate measuring device, which is the inner part of the milling and grinding machine tool, is employed to measure the surface error for aspheric mirror. As shown in Fig. 11b, four generatrices in the aspheric surface are tested in this work and they are fitted by the least square method. The average value of the four groups for surface error data is also calculated and fitted by the least square method.

The prediction results and the experimental results of surface error are shown in Fig. 12. The experimental results show that the surface error increases with the increase of rotation radius of workpiece, which is consistent with the prediction results of theoretical model. The prediction value of surface error model taking the wheel wear into account is closer to the experiment result comparing with that of surface error model without taking the wheel wear into account. The error between experiment results and the prediction model taking the wheel wear into account is within 20%, which indicates that the theoretical model of surface error for large-aperture aspheric mirror is reliable.

According to Fig. 12, the experimental values are larger than predicted values of theoretical model. Therefore, based on the experimental results, the original model can be modified by the correction coefficient K. Make $\sigma_{Experiment}=K\sigma_{Model}$, where $\sigma_{Experiment}$ is the experimental value and σ_{Model} is the predicted value of theoretical model.

The correction coefficient K can be solved by least square method. There are 26 groups of experimental value and predicted value, which are expressed as $(\sigma_{Experiment}(i), K\sigma_{Model}(i))$, where, $i = 1, 2, \ldots, 26$.

Make $\sigma_{\mathrm{Experiment}}(i) = K\sigma_{\mathrm{Model}}(i)$.

Residual error Q can be obtained by the following equation.

$$Q=\sum_{i=1}^{26}\left[\sigma_{\mathrm{Experiment}}(i)-\sigma_{\mathrm{Experiment}}(i)\right]^2=\sum_{i=1}^{26}\left[\sigma_{\mathrm{Experiment}}(i)-K\sigma_{\mathrm{Model}}(i)\right]^2 \quad (33)$$

When $\frac{\partial Q}{\partial K}=0$, the residual error is the smallest. And K is calculated as $K=\frac{\sum_{i=1}^{26}\sigma_{\mathrm{Experiment}}(i)}{\sum_{i=1}^{26}\sigma_{\mathrm{Model}}(i)}$ which is equal to 1.12.

$$\sigma=1.12\cdot\frac{\rho-\sqrt{(\rho-r)^2-\left(\frac{f}{2}\right)^2}-\sqrt{(r-\Delta r)^2-\left(\frac{f}{2}\right)^2}}{\cos\beta} \quad (34)$$

where

$$\begin{cases}\Delta r=\dfrac{a_p\cdot f\cdot x}{f\cdot x+15.9404\cdot v_s^{0.5577}\cdot a_p^{-0.1327}\cdot v^{-0.0882}\cdot(R+r\cdot\cos(\alpha+\beta))\cdot\sqrt{2\cdot a_p\cdot r\Big/\left(1-r/\rho\right)}}\\ \cos(\alpha+\beta)=\dfrac{\cos\alpha\sqrt{R_0^2-(1-e^2)x^2}-x\sin\alpha}{\sqrt{R_0^2+e^2x^2}}\\ \% \\ \rho=\dfrac{\left(e^2x^2+R_0^2\right)^{3/2}}{R_0^2}\\ \cos\beta=\dfrac{\sqrt{R_0^2-(1-e^2)x^2}}{\sqrt{R_0^2+e^2x^2}}\end{cases}$$

4 Conclusions

1. The spiral grinding method is chosen to grind large-aperture aspheric SiC mirror in this work. The surface error of large-aperture aspheric silicon carbide mirror is established based on residual height and radial wear of grinding wheel using the grinding ratio as a bridge.
2. The influence of grinding parameters on surface error is analyzed based on theoretical model. The results show that surface error increases with the increase of rotation radius of workpiece and feed velocity, while it decreases with the increase of rotation velocity of workpiece and arc radius of wheel. The influence of workpiece's rotation velocity and feed velocity of wheel is greater than that of rotation radius of workpiece and arc radius of wheel.
3. The regression equation of grinding ratio is established through grinding experiment, and correlation coefficient is 0.9774 which verifies the reliability of the regression equation. Furthermore, the complete formula of the surface error is acquired based on the regression equation of grinding ratio.
4. Finally, grinding experiment of large-aperture aspheric silicon carbide mirror is carried out on the five-axis NC milling and grinding machine tool of HZ-091 type, and the error between measured value of grinding experiment and prediction value of theoretical model is less than 20%, which indicates that the theoretical model is reliable.

Acknowledgments This work was supported by the National Key Basic Research and Development Program of China (973 program, Grant No.2011CB013202) and the National Key Research and Development Program of China (2016YFB1102204).

References

1. Kotani M, Imai T, Katayama H, Yui Y, Tange Y, Kaneda H, Enya K (2013) Quality evaluation of spaceborne SiC mirrors (II): evaluation technology for mirror accuracy using actual measurement data of samples cut out from a mirror surface. Appl Opt 52(26):6458–6466
2. Guo Y, Li Y, Lv B (2010) Design of new style unobscured three-mirror optical system. Acta Optical Sinica 30:1144–1147
3. Jiang X, Scott P, Whitehouse D (2007) Freeform surface characterization a fresh strategy. CIRP Ann-Manuf Techn 56(1):553–556

4. Kim B (2015) Development of aspheric surface profilometry using curvature method. Int J Precis Eng Man 16(9):1963–1968
5. Shimizu Y, Goto S, Lee J (2013) Fabrication of large-size SiC mirror with precision aspheric profile for artificial satellite. Precis Eng 37:640–649
6. Kumar RS, Shukla AK, Babu S, Sivakumar D, Gandhi AS (2011) Densification of silicon carbide using oxy-nitride additives for space-based telescope mirror applications. Opt Eng 50(7): 070504–070504
7. Ahn K, Rhee HG, Yang HS, Kihm H (2015) Silicon carbide deformable mirror with 37 actuators for adaptive optics. J of the Korean Phys Soc 67(10):1882–1888
8. Shen X, Dai Y, Deng H, Guan C, Yamamura K (2013) Comparative analysis of oxidation methods of reaction-sintered silicon carbide for optimization of oxidation-assisted polishing. Opt Express 21(22):26123–26135
9. Jiang Z, Yin Y, Wang Q, Chen X (2016) Predictive modeling of grinding force considering wheel deformation for toric fewer-axis grinding of large complex optical mirrors. J Manuf Sci E-T ASME 138(6):061008
10. Xie J, Li Q, Sun J, Li Y (2015) Study on ductile-mode mirror grinding of SiC ceramic freeform surface using an elliptical torus-shaped diamond wheel. J Mater Process Tech 222:422–433
11. Agarwal S (2016) Optimizing machining parameters to combine high productivity with high surface integrity in grinding silicon carbide ceramics. Ceram Int 42(5):6244–6262
12. Zhang F, Meng B, Geng Y, Zhang Y, Li Z (2016) Friction behavior in nanoscratching of reaction bonded silicon carbide ceramic with Berkovich and sphere indenters. Tribol Int 97:21–30
13. Ferreira PM, Liu CR (1993) A method for estimating and compensating quasistatic errors of machine tools. J Eng Ind 115(1):149–159
14. Chatterjee S (1997) An assessment of quasi-static and operational errors in NC machine tools. J Manuf Syst 16(1):59–68
15. Lin X, Guo Y, Wang Z, Xu Q (2013) Precision model and analysis of large axisymmetric aspheric grinding. Chin J Mech Eng 49(17): 65–72
16. Rahman MS, Saleh T, Lim HS, Son SM, Rahman M (2008) Development of an on-machine profile measurement system in ELID grinding for machining aspheric surface with software compensation. Int J Mach Tool Manu 48:887–895
17. Kuriyagawa T, Zahmaty MSS, Syoji K (1996) A new grinding method for aspheric ceramic mirrors. J Mater Process Tech 62(4): 387–392
18. Xiao M, Takamura T, Takahashi S, Takamasu K (2013) Random error analysis of profile measurement of large aspheric optical surface using scanning deflectometry with rotation stage. Precis Eng 37:599–605
19. Xi J, Zhao H, Li B, Ren D (2016) Profile error compensation in cross-grinding mode for large-diameter aspheric mirrors. Int J Adv Manuf Technol 83:1515–1523
20. Lin X, Wang Z, Guo Y, Peng Y, Hu C (2014) Research on the error analysis and compensation for the precision grinding of large aspheric mirror surface. Int J Adv Manuf Technol 71(1–4):233–239
21. Ding K, Fu Y, Su H, Gong X, Wu K (2014) Wear of diamond grinding wheel in ultrasonic vibration-assisted grinding of silicon carbide. Int J Adv Manuf Technol 71(9–12):1929–1938
22. Shanawaz AM, Sundaram S, Pillai UTS, Aurtherson PB (2011) Grinding of aluminium silicon carbide metal matrix composite materials by electrolytic in-process dressing grinding. Int J Adv Manuf Technol 57(1–4):143–150
23. Hwang Y, Kuriyagawa T, Lee SK (2006) Wheel curve generation error of aspheric microgrinding in parallel grinding method. Int J Mach Tool Manu 46(15):1929–1933
24. Stephen M (2008) Grinding technology: theory and applications of machining with abrasives. Industrial Press Inc., New York